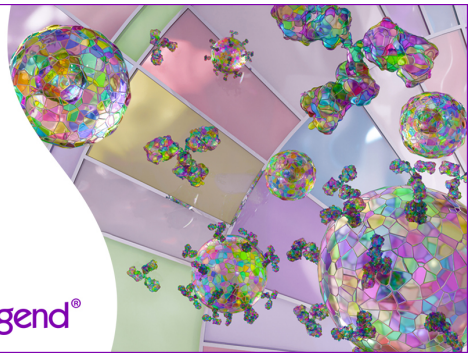

The Journal of Immunology
RESEARCH ARTICLE | MARCH 24 2023

mTOR Activation Underlies Enhanced B Cell Proliferation and Autoimmunity in *Prkcd*$^{G510S/G510S}$ Mice

Marion Moreews; ... et. al

J Immunol (2023) 210 (9): 1209–1221.
https://doi.org/10.4049/jimmunol.2200818

mTOR Activation Underlies Enhanced B Cell Proliferation and Autoimmunity in *Prkcd*$^{G510S/G510S}$ Mice

Marion Moreews,* Anne-Laure Mathieu,* Kevin Pouxvielh,* Quentin Reuschlé,† Annabelle Drouillard,* Pénélope Dessay,* Marie Meignien,*,‡ Jiang Zhang,* Lucie Fallone,* Noëmi Rousseaux,* Michelle Ainouze,* Amaury Rey,* Ommar Omarjee,* Elodie Decembre,* Vanina Lenief,* Sophia Djebali,* Olivier Thaunat,*,§,¶ Marlène Dreux,* Laurent Genestier,* Thierry Defrance,* Pauline Soulas-Sprauel,† Antoine Marçais,* Thierry Walzer,*,[1] and Alexandre Belot*,‡,[1]

Autosomal recessive *PRKCD* deficiency has previously been associated with the development of systemic lupus erythematosus in human patients, but the mechanisms underlying autoimmunity remain poorly understood. We introduced the *Prkcd* G510S mutation that we previously associated to a Mendelian cause of systemic lupus erythematosus in the mouse genome, using CRISPR-Cas9 gene editing. *Prkcd*$^{G510S/G510S}$ mice recapitulated the human phenotype and had reduced lifespan. We demonstrate that this phenotype is linked to a B cell–autonomous role of *Prkcd*. A detailed analysis of B cell activation in *Prkcd*$^{G510S/G510S}$ mice shows an upregulation of the PI3K/mTOR pathway after the engagement of the BCR in these cells, leading to lymphoproliferation. Treatment of mice with rapamycin, an mTORC1 inhibitor, significantly improves autoimmune symptoms, demonstrating in vivo the deleterious effect of mTOR pathway activation in *Prkcd*$^{G510S/G510S}$ mice. Additional defects in *Prkcd*$^{G510S/G510S}$ mice include a decrease in peripheral mature NK cells that might contribute to the known susceptibility to viral infections of patients with *PRKCD* mutations. *The Journal of Immunology*, **2023, 210: 1209–1221.**

Systemic lupus erythematosus (SLE) is a devastating autoimmune disease whose symptoms may include joint pain, fever, skin rash, and organ damage. SLE is currently incurable, and the therapeutic arsenal to treat SLE remains very limited, without specific treatment for the different clinical forms of the disease. SLE usually occurs in adults and less frequently in children (juvenile-onset SLE [jSLE]), but in the latter case it is usually more severe. In jSLE, genetics is thought to be a major contributing factor to the onset of the disease, and a subset of jSLE is driven by inborn errors of a single gene, defining the concept of monogenic SLE (1). Using next generation sequencing, we recently found that at least 7% cases of jSLE are in fact monogenic (1). Gene mutations may alter different immunological pathways, such as the clearance of apoptotic bodies (i.e., efferocytosis), the production of type I IFN (IFN-I), or B cell tolerance (2).

Mechanistically, SLE is caused by an aberrant immune response resulting in the production of inflammatory cytokines, such as IFN-I, and autoantibodies directed against components of apoptotic bodies (nucleosomes, chromatin, histones, etc.), as well as the formation and deposition of immune complexes responsible for tissue inflammation and damage (3). Autoantibodies identified in SLE are generally high-affinity, somatically mutated IgG, which suggests they have arisen in germinal centers (GCs), where T cells provide help to B cells for class switching and somatic mutation (3). They are produced by mature B cells, differentiated into plasma cells, secondary to a break in B cell tolerance. B cell tolerance ensures that B cells expressing BCRs with the ability to recognize self-antigens are either modified (BCR editing) or eliminated to avoid the development of autoimmunity. In particular, strong BCR signaling on engagement by self-antigens induces apoptosis of developing B cells (4).

*CIRI, Centre International de Recherche en Infectiologie, (Team LYACTS), Univ Lyon, Inserm, U1111, Université Claude Bernard Lyon 1, CNRS, UMR5308, ENS de Lyon, Lyon, France; †INSERM UMR-S1109, Department of Clinical Immunology and Internal Medicine, National Reference Center for Systemic Autoimmune Diseases, Tertiary Center for Primary Immunodeficiency, Faculty of Pharmacy, Université de Strasbourg, Strasbourg, France; ‡Hospices Civils de Lyon, Edouard Herriot Hospital, Immunology Laboratory, Lyon, France; §Department of Transplantation, Nephrology and Clinical Immunology, Edouard Herriot Hospital, Hospices Civils de Lyon, Lyon, France; and ¶Lyon-Est Medical Faculty, Claude Bernard University (Lyon 1), Lyon, France

Received for publication November 3, 2022. Accepted for publication February 21, 2023.

[1]T.W. and A.B. are cosenior authors.

ORCIDs: 0000-0002-5116-2443 (M. Moreews); 0000-0002-2893-7001 (A.-L.M.); 0000-0002-5344-8066 (Q.R.); 0000-0001-7188-7655 (A.D.); 0000-0002-5404-7555 (M. Meignien); 0000-0001-7392-8270 (J.Z.); 0000-0002-7152-1300 (N.R.); 0000-0002-6928-932X (M.A.); 0000-0002-6355-7119 (A.R.); 0000-0002-0567-5387 (S.D.); 0000-0002-3648-8963 (O.T.); 0000-0002-6607-4796 (M.D.); 0000-0002-0527-4583 (L.G.); 0000-0002-6943-358X (T.D.); 0000-0002-2058-4811 (P.S.-S.); 0000-0002-3591-6268 (A.M.); 0000-0002-0857-8179 (T.W.); 0000-0003-4902-5332 (A.B.).

This work was supported by the Agence Nationale de la Recherche (ANR JCJC to A.B.), Fondation pour la Recherche Médicale (FDT202106012999), and institutional grants from INSERM, CNRS, Université Lyon I, and ENS de Lyon.

M. Moreews designed, performed, and analyzed experiments. A.-L.M. performed experiments and analyzed the data. K.P., Q.R., A.D., P.D., M. Meignien, J.Z., L.F., N.R., M.A., A.R., O.O., E.D., V.L., and S.D. provided technical assistance for some experiments. O.T., M.D., L.G., T.D., P.S.-S., and A.M. provided conceptual input for some of the experiments and help for writing the manuscript. T.W. and A.B. designed the study, analyzed the data, and wrote the manuscript. M. Moreews prepared the initial draft. T.W. and A.B. reviewed and finalized the paper.

Address correspondence and reprint requests to Dr. Thierry Walzer and Prof. Alexandre Belot, Centre International de Recherche en Infectiologie (CIRI), INSERM U1111–CNRS UMR5308, Université Lyon 1, ENS de Lyon, 21 Avenue Tony Garnier, 69365 Lyon Cedex 07, France. E-mail addresses: thierry.walzer@inserm.fr (T.W.) and alexandre.belot@chu-lyon.fr (A.B.)

The online version of this article contains supplemental material.

Abbreviations used in this article: ABC, aging-associated B cell; ANA, antinuclear Ab; BM, bone marrow; CTV, CellTrace Violet; DC, dendritic cell; DEG, differentially expressed gene; GC, germinal center; IFN-I, type I IFN; ISG, IFN-stimulated gene; jSLE, juvenile-onset systemic lupus erythematosus; LN, lymph node; MHCII, MHC class II; MZ, marginal zone; PBES, Plateau de Biologie Expérimentale de la Souris; PIP3, phosphatidylinositol (3,4,5)-trisphosphate; PKC-δ, protein kinase C-δ; RALD, Ras-associated lymphoproliferative disease; RF, rheumatoid factor; SLE, systemic lupus erythematosus; WT, wild-type.

Consequently, mutations in genes affecting the strength or the quality of BCR signal transduction can cause B cell tolerance breakdown and autoimmunity, as previously reviewed (4, 5).

We and others previously identified *PRKCD* mutations in jSLE patients (6–12). *PRKCD* encodes for protein kinase C-δ (PKC-δ), a cytosolic kinase of the novel diacylglycerol-dependent and calcium-independent serine/threonine PKC group. In our own study, we described a homozygous mutation (c.1528G>A, p.G510S) of the *PRKCD* gene in three jSLE patients from the same family (6). The causality of these mutations in SLE was supported by genetic analyses and by previous observations of a lupus phenotype in *Prkcd*$^{-/-}$ mice (13, 14). Moreover, multiple other mutations in *PRKCD* were associated with jSLE since the original observations (8–12). The G510S missense mutation affects a highly conserved amino acid of the protein activation loop and is associated with a low, but not abrogated, PKC-δ expression (6). We also demonstrated that the mutated protein displays a reduced activity, and that it was refractory to stimulation by PMA. PKC-δ is broadly expressed and plays multiple roles in cells of the innate and adaptive immune systems. For example, PKC-δ regulates neutrophil migration and oxidative burst (15, 16) and also influences macrophage effector functions (17). T cell proliferation and cytokine production are slightly increased in *Prkcd*$^{-/-}$ mice after TCR triggering (13). In B cells, PKC-δ is phosphorylated after BCR engagement (18, 19) and is involved in BCR signaling. A previous study proposed that PKC-δ amplified the Ca^{2+}-dependent Ras/Erk pathway, thereby inducing apoptosis of autoreactive transitional B cells (20). Another study showed that PKC-δ translocation into the nucleus was a proapoptotic event that could be prevented by BAFF signaling (21). PKC-δ nuclear translocation was recently shown to occur in GC B cells, downstream of sphingomyelin synthase 2 (22). Overall, several lines of evidence point to PKC-δ as an important regulator of B cell tolerance, and the proposed mechanism involved the induction of apoptosis in immature cells. Yet, most studies have used *Prkcd*$^{-/-}$ mice as a disease model, which may not adequately model SLE pathogenesis in patients with *PRKCD* mutations. To address this issue, we generated a knock-in mouse strain bearing the *Prkcd* G510S mutation. Our results showed that *Prkcd*$^{G510S/G510S}$ mice developed a strong autoimmune phenotype recapitulating the disease observed in patients. We hypothesized that B cells were the major drivers of the disease. We performed a detailed analysis of their phenotype and of their response to BCR engagement to tackle this question and to find a specific treatment for the disease.

Materials and Methods

Mice

Prkcd$^{G510S/G510S}$ mice were generated using CRISPR-Cas9 gene editing. guide RNA and single-stranded oligodeoxynucleotides were designed using CRISPOR (Tefor) and Mainworkbench softwares (Qiagen) and were synthesized by Eurogentec. Mouse zygotes were electroporated with ribonucleoprotein complex in our animal facility (Plateau de Biologie Expérimentale de la Souris [PBES]), as previously described (23). Littermate mice were backcrossed three times to C57BL/6 mice, purchased from Charles River Laboratories (L'Arbresle). Mice were bred and maintained under specific pathogen-free conditions in the PBES. Age-matched (8–20 wk old) and sex-matched littermate mice were used as controls. This study was carried out in accordance with the French recommendations in the Guide for the Ethical Evaluation of Experiments Using Laboratory Animals and the European guidelines 86/609/CEE. The local bioethics committee (Comité d'Éthique en Expérimentation Animale de la Région Rhône-Alpes) approved all experimental studies.

Generation of bone marrow chimeras

For the generation of mixed bone marrow chimeras, donor-derived BM cells of the indicated genotypes (CD45.2^{+}) were mixed with BM cells from Ly5a (CD45.1) mice and transferred i.v. into sublethally (10 Gy) irradiated Ly5axC57BL/6 (CD45.1, CD45.2) recipients. Mice were analyzed 8–12 wk after BM reconstitution. For the generation of μMT: *Prkcd*$^{+/+}$ and μMT: *Prkcd*$^{G510S/G510S}$ mixed BM chimeras, a 4:1 ratio of donor-derived BM cells from μMT mice and *Prkcd*$^{+/+}$ or *Prkcd*$^{G510S/G510S}$ mice was transferred i.v. into sublethally (10 Gy) irradiated Ly5axC57BL/6 (CD45.1, CD45.2) recipients.

Rapamycin treatment

Mice were treated with either vehicle: PBS 1× (Life Technologies) or Rapamune (rapamycin; Pfizer) (2 mg/kg/d) by gavage during 28 d. Blood sampling from the retro-orbital sinus was performed before and after treatment to analyze antinuclear autoantibodies and IFN-stimulated gene (ISG) expression.

Antinuclear Ab assays

Antinuclear Abs (ANAs) reactivity were detected by indirect immunofluorescence staining of HEp-2 cell slides (Bio-Rad) using sera from indicated mice at a 1:50 dilution and probed with FITC-conjugated goat anti-murine IgG $F(ab')_2$ (ImmunoJackson Research). All images were obtained with a Nikon Eclipse T&2R (Nikon) microscope and were analyzed using ImageJ (National Institutes of Health). For each experiment, the fluorescence intensity of 10 nuclei in each micrograph was quantified and normalized to the value obtained using an ANA-positive serum.

ELISA

Total murine IgG or IgM serum levels were measured as follows. In brief, 96-microwell plates (Nunc Maxisorp; ThermoFisher) were coated with purified goat anti-mouse IgG or IgM (Jackson ImmunoResearch) in carbonate buffer (Na2CO3 0.1 M, NaHCO3 0.1 M, pH 9.5) for 1 h at 37°C, and total IgG or IgM were detected with HRP-conjugated goat anti-mouse γ or μ (Jackson ImmunoResearch). Levels of Ig were determined by comparison with a standard curve using purified IgG or IgM (Jackson ImmunoResearch). Serum anti-dsDNA and rheumatoid factor (RF) activities were analyzed as follows. In brief, 96-microwell plates (Nunc Maxisorp; ThermoFisher) were coated with purified Calf-Thymus DNA at 100 ng/ml (Sigma-Aldrich) in Tris-HCl buffer (Tris HCl 50 mM, EDTA 10 mM, pH 7.5) for 1 h at 37°C. Then, ssDNA was digested with S1 nuclease at 0.001 U/μl (Promega) in acetate buffer (50 mM Na acetate, 50 mM NaCl, 1 mM ZnSO4, 5% glycerol, pH 4.5) for 1 h at 37°C. For RF detection, 96 microwell plates (Nunc Maxisorp; ThermoFisher) were coated with purified mouse IgG at 50 μg/ml (Jackson Immunoresearch) in carbonate buffer (Na2CO3 0.1 M, NaHCO3 0.1 M, pH 9.5) for 1 h at 37°C. Serum samples were incubated at several dilution overnight at room temperature. Plates were then incubated with HRP-conjugated goat anti-mouse γ or μ (Jackson ImmunoResearch) for 1 h at 37°C. For all ELISA tests, the wells were developed with Fast Ortho-Phenylene Diamine substrate (Sigma-Aldrich). The reaction was stopped with addition of H2SO4 solution (1 M) after 20 min at room temperature, and absorbance was measured at 490 nm.

IFN score

RNA was extracted from whole blood with Direct-zol RNA MicroPrep (Ozyme), and cDNA was generated using the high-capacity RNA-to-cDNA kit (Applied Biosystems). PCR was carried out with a FastStart Universal SYBR Green Master (Roche) on a StepOne plus instrument (Applied Biosystems). Primers were designed using the Roche software. The following primers were used for quantitative PCR: MM-ISG15-F, 5′-AAGCAGCCAGAAGCAGACTC-3′; MM-ISG15-R, 5′-CACGGACACCAGGAAATCGT-3′; MM-IFIT1-F, 5′-AAGGCACTGAACAACAAGACC-3′; MM-IFIT1-R, 5′-TGACTGCTTATGAAACTGTAGGAAA-3′; MM-RSAD2-F, 5′-GTGGACGAAGACATGAATGAAC-3′; MM-RSAD2-R, 5′-CTCAATTAGGAGGCACTGGAA-3′; MM-GAPDH-F, 5′-GCATGGCCTTCCGTGTTC-3′; MM-GAPDH-R, 5′-TGTCATCATACTTGGCAGGTTTCT-3′. The expression of ISGs was normalized to the level of GAPDH, and the IFN score was calculated as the median of the normalized count of the three ISGs.

Kidney histopathology

Kidneys were fixed in 10% neutral buffered formalin and embedded in paraffin. Kidney sections were cut at 5 μm thickness for H&E staining (Sigma-Aldrich). All images were obtained with an Axioimager Z1 microscope (Zeiss) and Coolsnap camera using MetaMorph software (Molecular Devices).

Proteinuria measurement

Urine was collected from mice and deposited on an Albustix strip (Siemens). Proteinuria score was determined as follows: 0 = negative; 1 = trace; 2 = 30 mg/dl; 3 = 100 mg/dl; 4 = 300 mg/dl; and 5 = >2000 mg/dl.

Immunofluorescence analysis

Mouse kidneys were embedded in OCT and snap frozen over liquid nitrogen. Six-micrometer thin sections were cut on a cryostat, mounted on SuperFrost Plus Gold slides (Thermo Fisher Scientific), and fixed in cold acetone for 20 min. Kidney sections were saturated with BSA 1% and donkey serum 5% blocking solution during 30 min, then with BSA 1% blocking solution containing anti-CD16/CD32 (BD Biosciences) during 30 min and were stained using FITC-anti-IgG (Jackson Immunoresearch) or FITC-anti-IgM (Jackson Immunoresearch). The images of stained kidney sections were captured using Axioimager Z1 microscope (Zeiss) and Coolsnap camera using MetaMorph software (Molecular Devices) and were analyzed using ImageJ (National Institutes of Health).

Automated Western immunoblotting

Cells were lysed in radioimmunoprecipitation lysis buffer (25 mM Tris, HCl, pH 7.4, 150 mM NaCl, 1% Nonidet P-40, 1% sodium deoxycholate, and 0.1% SDS containing protease and phosphatase inhibitors; Sigma-Aldrich) for 30 min at 4°C. Supernatant was collected after centrifugation at 16,000 × *g*, 4°C, and protein content was quantified using the μBCA quantification kit (Thermo Fisher Scientific). PKC-δ protein expression was detected using the automated Jess Simple Western system (ProteinSimple). In brief, cell lysates were diluted to 0.5 μg/μl in 0.1× sample buffer and Fluorescent 5× Master mix containing 400 mM DTT (ProteinSimple). Samples were denatured at 95°C for 5 min, and proteins were separated in capillaries using a 12- to 230-kDa Jess separation module and following the manufacturer's standard method (ProteinSimple). Anti–PKC-δ (Cell Signaling Technology) was used for protein detection and revealed using HRP-coupled secondary Abs (ProteinSimple). Digital image of chemiluminescence of the capillary was analyzed using Compass Simple Western software (version 4.1.0; Protein Simple) that calculated automatically height (chemiluminescence intensity), area, and signal/noise ratio. PKC-δ level was normalized on total protein expression, using the JESS protein Normalization assay and according to manufacturer's instructions.

Flow cytometry

Single-cell suspensions of BM, lymph node (LN), and spleens were stained with Ab cocktails. The following mAbs from eBioscience, BD Biosciences, or BioLegend were used for flow cytometry: anti-CD19 (6D5), anti-B220 (RA3-6B2), anti-CD3 (145-2C11, 500A2), anti-CD8a (53-6.7), anti-CD4 (GK1.5), anti-NK1.1 (PK136), anti-CD11b (M1/70), anti-CD11c (N418), anti-IgM (R6-60.2), anti-IgD (11-26c.2a), anti-IgG1 (A85-1), anti-CD21 (7E9), anti-CD23 (B3B4), anti-CD24 (M1/69), anti-CD27 (LG.7F9), anti-CD45.1 (A20), anti-CD45.2 (104), anti-CD64 (X54-5/7.1), anti-CD69 (H1.2F3), anti-CD86 (GL1), anti-CD95 (Jo2), anti-CD138 (281-2), anti-CD317 (927), anti-TACI (8F10), anti-MHC class II (MHCII; M5/114.15.2), anti-GL7 (GL7), anti-KI67 (solA15), anti-Ly6C (HK1.4), anti-Ly6G (RB6-8C5), anti–Siglec F (E50-2440), anti–Siglec H (440c), anti-F4/80 (T45-2342), and anti-CD107a (1D4B). Intracellular stainings and stainings for phosphorylated proteins were performed using the Foxp3 fixation/permeabilization or Lyse/Fix and Perm-III kits (BD Bioscience). The following Abs from eBioscience, BD Biosciences, BioLegend, and Tube-Bio were used for intracellular staining and phospho-specific flow cytometry: anti–P-Syk (pY348) (I120-722), anti–P-Btk (pY223) (N35-86), anti–p-Akt (pS473) (M89-61), anti–p-Erk (T202/pY204) (201), anti–p-S6 (p240/244) (D57.2.2E), anti–P-4E-BP1 (Thr37/46) (236B4), anti–T-bet (4B10), and anti–phosphatidylinositol (3,4,5)-trisphosphate (PIP3) (Z-P345). Cell viability was measured by staining with the fixable viability dye eFluor 506 or Near IR (Thermo Fisher Scientific). Flow cytometry was carried out on a FACS Fortessa (Becton-Dickinson). Data were analyzed using FlowJo (Treestar).

In vitro B cell apoptosis experiments

A total of 2×10^6 splenocytes were cultured in complete medium (RPMI-1640 supplemented with 10% heat-inactivated FCS, 10 mM Hepes, 1 mM sodium pyruvate, and 50 μM 2-ME). After 48 or 72 h, B cells viability was assessed by flow cytometry.

In vitro B cell stimulation experiments

Splenocytes were labeled with 5 μM CellTrace Violet (CTV) dye (Thermo Fisher Scientific) in PBS for 20 min at 37°C. After washing with complete medium (RPMI-1640 supplemented with 10% heat-inactivated FCS, 10 mM Hepes, 1 mM sodium pyruvate, and 50 μM 2-ME), cells were seeded at a density of 2×10^6 cells in 1 ml of stimulation medium containing 10 μg/ml AffiniPure F(ab′)$_2$ Fragment Goat Anti-Mouse IgM, μ chain specific (Jackson Immunoresearch) and 5 μg/ml CD40 (mouse) mAb (FGK45). At day 3, proliferation of stimulated B cells was assessed by flow cytometry.

For the measurement of phosphorylated proteins, different CD45 Abs or CTV dye (Thermo Fisher Scientific) dilutions were used to barcode splenocytes from the indicated genotypes after 1 h at 4°C. Next, barcoded cells of each genotype were pooled and incubated for 15 min at 4°C with 10 μg/ml AffiniPure F(ab′)$_2$ Fragment Goat Anti-Mouse IgM, μ chain specific (Jackson Immunoresearch), then with 10 μg/ml Rabbit anti-Goat IgG (H+L), Superclonal Recombinant Secondary Ab (Thermo Fisher Scientific) for 15 min. In some experiments, some inhibitors were used at the following concentrations: cerdulatinib (20 nM; Sigma-Aldrich), PRT062607 (11.11 nM; Sigma-Aldrich), wortmannin (37 nM; Sigma-Aldrich), and rapamycin (1.85 nM; Merck). Splenocytes were incubated at 37°C for the stimulation and fixed by addition of 10 vol of Lyse/Fix at the indicated time point.

In vitro stimulation of NK cells

Spleen cell suspensions were incubated with biotinylated mAbs against CD3 (14–2C11), TCRβ (H57-597), TCRγδ (GL3), CD19 (ebio1D3), and TER-119 (ter119) (eBioscience), followed by incubation with anti-biotin microbeads (Miltenyi) and NK cell enrichment by magnetic separation using the AutoMACS device (Miltenyi). Enriched NK cells were cocultured for 4 h with YAC-1 cells at 1:1 ratio calculated based on the cell number and the percentage of NK cells after purification. The expression of surface CD107a was then measured on NK cells by flow cytometry.

RNA sequencing

Follicular B cells $CD3^-CD19^+CD45R^+CD24^{int}CD21^{int}CD23^+$ were sorted using a FACSAria Cell Sorter (Becton-Dickinson). Purity of sorted cell populations was >98% as measured by flow cytometry. FO B cells were stimulated with 10 μg/ml AffiniPure F(ab′)$_2$ Fragment Goat Anti-Mouse IgM, μ chain specific (Jackson Immunoresearch) during 4 h. RNA libraries were prepared as follows. In brief, total RNA was purified using the Direct-Zol RNA microprep kit (Zymo Research) according to the manufacturer's instructions and was quantified using QuantiFluor RNA system (Promega). The preparation of library was performed using the SENSE mRNA-Seq Library Prep Kit (Lexogen) according to the manufacturer's instructions. Tagged library quality was checked on D1000 screen tape and analyzed on Tape station 4200 (Agilent). Sequencing was performed by the GenomEast platform, a member of the "France Génomique" consortium (ANR-10-INBS-0009), on an Illumina HiSeq 4000 sequencing machine (read length 1×50 nt).

Statistical analysis

Statistical analysis was performed with GraphPad Prism 6 software. We used unpaired Student *t* test or Mann–Whitney test to calculate statistical significance when comparing a single parameter between two experimental groups. If more than one parameter (sex or cell subsets) was compared, a false discovery rate adjustment was applied. One-way ANOVA was used when more than two experimental groups were compared, and the statistical significance was determined using Tukey's post hoc test. Two-way ANOVA with Bonferroni multiple comparison correction was used when comparing two parameters between more than two experimental groups.

Results

Prkcd$^{G510S/G510S}$ *mice develop a severe lupus phenotype*

PRKCD mutations result in a highly variable clinical phenotype, which may result from differences in the level of expression or residual activity of the protein (6–12, 16, 24–26) (summarized in Supplemental Table I). To investigate the immunological mechanism underlying autoimmunity in patients with the PRKCD G510S mutation (6), we generated a knock-in mouse strain bearing the *Prkcd* G510S mutation using CRISPR-Cas9 genome editing (Fig. 1A). Capillary electrophoresis analysis showed that *Prkcd*$^{G510S/G510S}$ mice had decreased expression of PKC-δ at the protein level in various lymphoid organs, such as spleen, thymus, and BM, compared with control mice (Fig. 1B), which suggests a similar impact of the *PRKCD* mutation on protein expression in mouse and human (6). *Prkcd*$^{G510S/G510S}$ mice had a reduced lifespan compared with *Prkcd*$^{+/G510S}$ and *Prkcd*$^{+/+}$ control mice (Fig. 1C). Indeed, all *Prkcd*$^{G510S/G510S}$ mice died before the age of 48 wk, whereas ~80% of control mice (*Prkcd*$^{+/G510S}$ and *Prkcd*$^{+/+}$) were still alive at this age. Notably, *Prkcd*$^{G510S/G510S}$

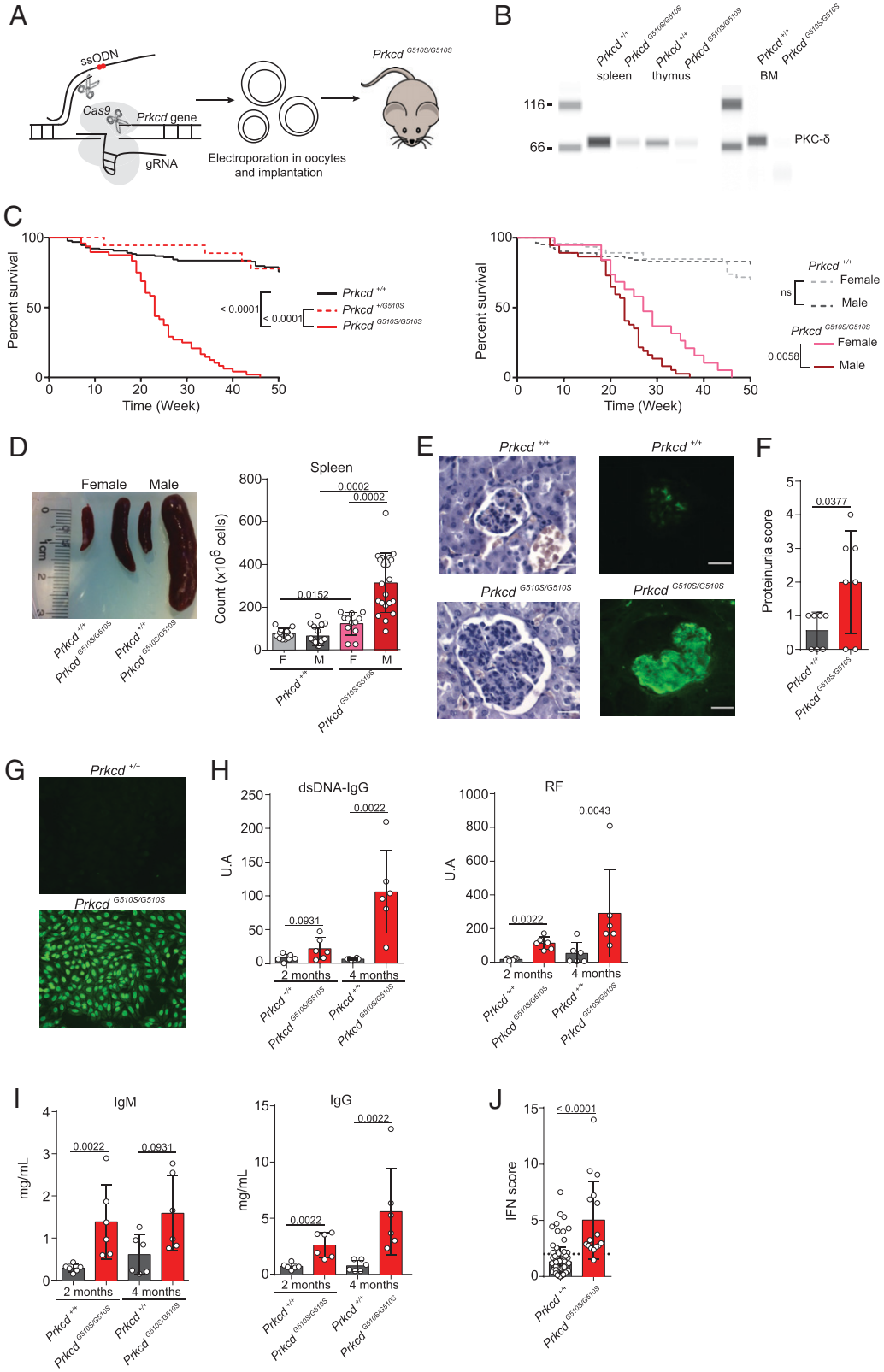

FIGURE 1. Autoimmune phenotype in *Prkcd*$^{G510S/G510S}$ mice. (**A**) Cartoon showing the method used to generate *Prkcd*$^{G510S/G510S}$ mice using CRISPR-Cas9–mediated genome editing. (**B**) Capillary electrophoresis analysis of PKC-δ expression in lymphoid organs of the indicated mice (representative of two independent experiments). (**C**) Survival curves of *Prkcd*$^{+/+}$ (n = 126), *Prkcd*$^{+/G510S}$ (n = 20), and *Prkcd*$^{G510S/G510S}$ (n = 43) mice (left: all sexes combined; right: sex indicated; *Prkcd*$^{+/+}$ female, n = 45, male, n = 81; *Prkcd*$^{G510S/G510S}$ female, n = 8, male, n = 35). Statistical test: Mantel–Cox. (**D**) Spleen size and cellularity in *Prkcd*$^{+/+}$ (female, n =12; male, n = 19) and *Prkcd*$^{G510S/G510S}$ (female, n =12; male, n = 19) mice aged 8–20 wk. Statistical test: Mann–Whitney test using false discovery rate adjustment. (**E**) Microscopy analysis of kidney inflammation. H&E staining (left) and anti–mouse IgG staining (right) of kidney sections (original magnification ×40) from mice aged 20 wk. (**F**) Proteinuria in mice aged 20–24 wk (n = 7) as measured using Albustix dipstick. Statistical test: Mann–Whitney. (**G**) Detection of ANAs by labeling Hep2 cells with serum from the indicated mice. (**H**) Quantification of dsDNA-IgG, RF, and (**I**) total IgM and *(Figure legend continues)*

males died slightly earlier than *Prkcd*$^{G510S/G510S}$ females. To address the causes of this premature death, we then carried out a clinical, biological, and histological examination of knock-in mice in comparison with controls. Spleens and LNs were significantly enlarged in *Prkcd*$^{G510S/G510S}$ mice, especially in males (Fig. 1D, Supplemental Fig. 1A). Kidneys from *Prkcd*$^{G510S/G510S}$ mice and not controls exhibited extensive infiltration in the glomeruli, which correlated with the presence of IgG deposit and proteinuria (Fig. 1E, 1F, Supplemental Fig. 1B). ANA, a hallmark of SLE, were already detected at 2 mo of age in *Prkcd*$^{G510S/G510S}$ mice (Fig. 1G). Moreover, ELISA assays revealed the presence of anti-dsDNA IgG, anti-dsDNA IgM, and RF in the serum of *Prkcd*$^{G510S/G510S}$ mice, and their levels increased with time except for anti-dsDNA IgM (Fig. 1H, Supplemental Fig. 1C). In addition, total IgG and IgM concentrations were strongly increased (Fig. 1I). We also monitored the expression of several ISGs in blood cells, because the production of IFN-I is often elevated in SLE patients. We calculated an IFN score, following a method previously used for human cells (27). This score was significantly higher in *Prkcd*$^{G510S/G510S}$ mice compared with controls (Fig. 1J). In addition, we found no difference between males and females in features related to autoimmunity i.e., autoantibodies, Ig levels, and IFN score (Supplemental Fig. 2A, 2B).

Overall, *Prkcd*$^{G510S/G510S}$ mice develop an early-onset and severe autoimmune phenotype combining lymphoproliferation, kidney failure, various autoantibodies, and positive IFN score, leading to premature death. This phenotype recapitulates clinical features observed in SLE patients bearing the *PRKCD* G510S mutation, validating our translational approach.

Impaired NK cell homeostasis in Prkcd$^{G510S/G510S}$ *mice*

To gain insight into the immunological mechanism leading to SLE in *Prkcd*$^{G510S/G510S}$ mice, we performed a large-scale flow cytometry analysis of immune subsets in these mice in comparison with controls. Because *Prkcd expression* is particularly high in myeloid cells (Supplemental Fig. 3), we first focused our analysis on innate immune cells. Macrophages, neutrophils, eosinophils, plasmacytoid dendritic cells (DCs) and conventional DCs were observed at similar frequencies in the spleen of *Prkcd*$^{G510S/G510S}$ mice and control mice, and no further investigations were performed for these subsets (Fig. 2A). By contrast, the frequency of NK cells was reduced 3-fold in the spleen of *Prkcd*$^{G510S/G510S}$ mice compared with controls. The absolute number of NK cells was similar in both mouse genotypes because of the splenomegaly in *Prkcd*$^{G510S/G510S}$ mice (Supplemental Fig. 4A). Nevertheless, we observed that *Prkcd*$^{G510S/G510S}$ NK cells had a bigger size and higher Ki67 expression than control NK cells (Supplemental Fig. 4B, 4C). Furthermore, *Prkcd*$^{G510S/G510S}$ NK cells displayed defective maturation with an increase of immature CD11b^{-}CD27^{+} cells and a decrease of mature CD11b^{+}CD27^{-} cells (Supplemental Fig. 4D). We stimulated spleen cells with YAC-1 cells that are classical NK cell targets. We observed higher cell surface expression of the cytotoxic marker CD107a cell surface expression after stimulation in *Prkcd*$^{G510S/G510S}$ NK cells than in control NK cells (Supplemental Fig. 4E). To test whether this NK cell phenotype was due to a cell-intrinsic impact of the *Prkcd* mutation or to the inflammatory environment, we generated mixed BM chimeric mice by reconstituting lethally irradiated Ly5a × C57BL/6 (CD45.1 × CD45.2) with a 1:1 mixture of BM from *Prkcd*$^{G510S/G510S}$ or *Prkcd*$^{+/+}$ (CD45.2) mice and Ly5a mice (CD45.1), taking advantage of CD45.1- and CD45.2-specific Abs to identify cells of the different genotypes. In wild-type (WT)/*Prkcd*$^{G510S/G510S}$ BM chimeric mice, a lower percentage of NK cells was found in spleen cells from the *Prkcd*$^{G510S/G510S}$ genotype compared with the WT genotype (Supplemental Fig. 4F), and their maturation was also impaired (Supplemental Fig. 4G). However, the degranulation capacity of *Prkcd*$^{G510S/G510S}$ NK cells was similar to that of WT counterparts in mixed BM chimeras (Supplemental Fig. 4H). Altogether, these results show a cell-intrinsic impact of the *Prkcd*$^{G510S/G510S}$ mutation on NK cell development and homeostasis, whereas the impact on degranulation capacities is probably cell extrinsic.

B cell homeostasis is altered in Prkcd$^{G510S/G510S}$ *mice*

Next, we examined adaptive lymphocyte features in *Prkcd*$^{G510S/G510S}$ mice in comparison with controls. As shown in Fig. 2A, we observed a decreased frequency of CD8 T cells and a normal frequency of CD4 T cells in the spleen of *Prkcd*$^{G510S/G510S}$ mice compared with controls. The proportion of B cells was similar in the BM and spleen of *Prkcd*$^{G510S/G510S}$ and control mice, but this proportion was higher in the LNs of *Prkcd*$^{G510S/G510S}$ mice than in controls. B cell size was higher in *Prkcd*$^{G510S/G510S}$ mice than in controls, irrespective of the organ analyzed (Fig. 2B), suggesting ongoing activation. In agreement with this hypothesis, peripheral *Prkcd*$^{G510S/G510S}$ B cells expressed significantly higher levels of activation markers CD69, MHCII, and CD86 and proliferation marker Ki67 than control B cells (Fig. 2C, Supplemental Fig. 5A). We then performed a detailed analysis of immature and mature B cell subsets. The frequencies of precursor, immature, transitional, and mature B cells in the BM were similar in *Prkcd*$^{G510S/G510S}$ and control mice (Fig. 2D), and so were the proportions of transitional and follicular B cells in the spleen of both strains (Fig. 2E, 2F). However, marked differences were observed for other B cell subsets. In particular, the proportion of marginal zone (MZ) B cells was strongly reduced, whereas the proportions of GC and plasma cells (PC) were elevated in the spleen of *Prkcd*$^{G510S/G510S}$ compared with control mice (Fig. 2F, 2G). We then inspected aging-associated B cells (ABCs) defined as CD3^{-}CD19^{+}B220^{+} IgM^{+}CD11b^{+}CD11c^{+}T-bet^{+}. This population is known to expand with age and in SLE patients (28). We observed an elevated proportion of these cells in the spleen of *Prkcd*$^{G510S/G510S}$ mice (Fig. 2G). Notably, PC and MZ B cells had an increased Ki67 expression in *Prkcd*$^{G510S/G510S}$ mice compared with controls (Supplemental Fig. 5B). Overall, the analysis of activation markers and peripheral B cell subsets in *Prkcd*$^{G510S/G510S}$ mice is evocative of B cell–driven autoimmunity.

To test whether this phenotype was intrinsically caused by the *Prkcd* mutation in B cells, we analyzed the B cell compartment in the spleen of BM chimeras described earlier. In WT/*Prkcd*$^{G510S/G510S}$ chimeric mice, *Prkcd*$^{G510S/G510S}$ splenic B cells had a clear competitive advantage over control B cells (Fig. 2H), whereas no difference in B cell proportion was observed between CD45.1 and CD45.2 genotypes in WT/*Prkcd*$^{+/+}$ chimeric mice. Moreover, *Prkcd*$^{G510S/G510S}$ B cells had an activated phenotype in chimeric mice, as shown by a high expression level of activation markers (Fig. 2I), and among *Prkcd*$^{G510S/G510S}$ B cells, PCs and ABCs were overrepresented compared with controls (Fig. 2J). These results indicate a cell-intrinsic role of the *Prkcd*$^{G510S/G510S}$ mutation in B cells, leading to

IgG as measured by ELISA in the serum of mice of the indicated age. For each group, $n = 6$; statistical test: Mann–Whitney. (**J**) IFN score in blood cells of the indicated mice aged 8–16 wk ($n = 29$). Statistical test: unpaired *t* test. Scale bars, 20 μm. Data are presented as the mean ± SD; no marks indicate lack of statistical significance.

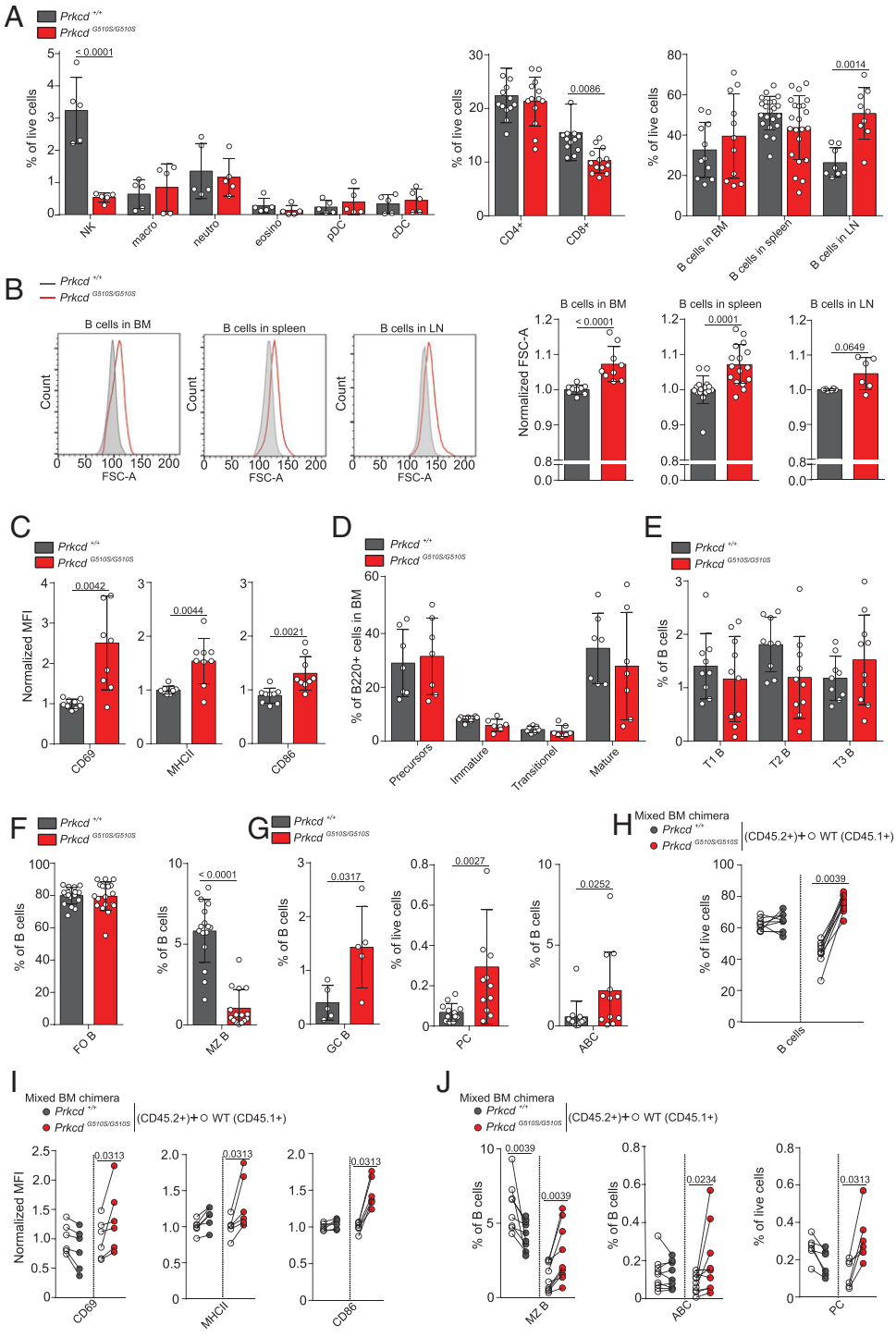

FIGURE 2. Alteration of immune cell populations in *Prkcd*$^{G510S/G510S}$ mice. (**A**) Flow cytometry analysis of NK cells, macrophages, neutrophils, eosinophils, plasmacytoid DCs (pDCs), and conventional DCs (cDCs) (left histogram, $n = 5$), CD4$^+$ and CD8$^+$ T cells (middle histogram, $n = 13$), or B cells (right histogram $n = 9–22$). Data show the percentages of indicated subsets among live cells in cell suspensions from spleen (left and middle) or indicated organs (right) of *Prkcd*$^{+/+}$ and *Prkcd*$^{G510S/G510S}$ mice aged 12–20 wk. Statistical test: Mann–Whitney. (**B**) Flow cytometry analysis of B cell forward scatter-A in BM, spleen, and LN of the indicated mice aged 12–20 wk. Left, Representative FACS panels; right, dot plots showing normalized mean forward scatter-A in different experiments. Statistical test: Mann–Whitney. (**C**) Normalized mean fluorescence intensity (MFI) of CD69, MHCII, and CD86 staining in gated B cells from the spleen of the indicated mice aged 20 wk, as measured by flow cytometry ($n = 9$ in three independent experiments, MFI relative to WT levels). Statistical test: Mann–Whitney. (**D–G**) Flow cytometry analysis of the frequency of indicated B cells subsets in the BM ($n = 7$) (D) or spleen ($n = 5–19$) (E–G) of the indicated mice aged 12–20 wk. Statistical test: Mann–Whitney. (**H–J**) Flow cytometry analysis of mixed BM chimeras, reconstituted with a 1:1 mixture of BM from CD45.1$^+$ WT mice and BM from CD45.2$^+$ mice (WT or *Prkcd*$^{G510S/G510S}$ mice as indicated). The following parameters were analyzed: (H) frequency of total B cells among cells of the indicated genotype; (I) MFI of CD69, MHCII, and CD86 staining in gated B cells of the indicated genotype; (J) frequency of MZ B cells, ABCs, and PC cells in total B cells of the indicated genotype. Statistical test: Wilcoxon matched-pairs signed rank. Lines connect data obtained for the same chimeric mice. Chimeric mice ($n = 6–9$ for each combination) were analyzed 8–12 wk posttransplantation. Data are presented as the mean ± SD; no mark indicates lack of statistical significance.

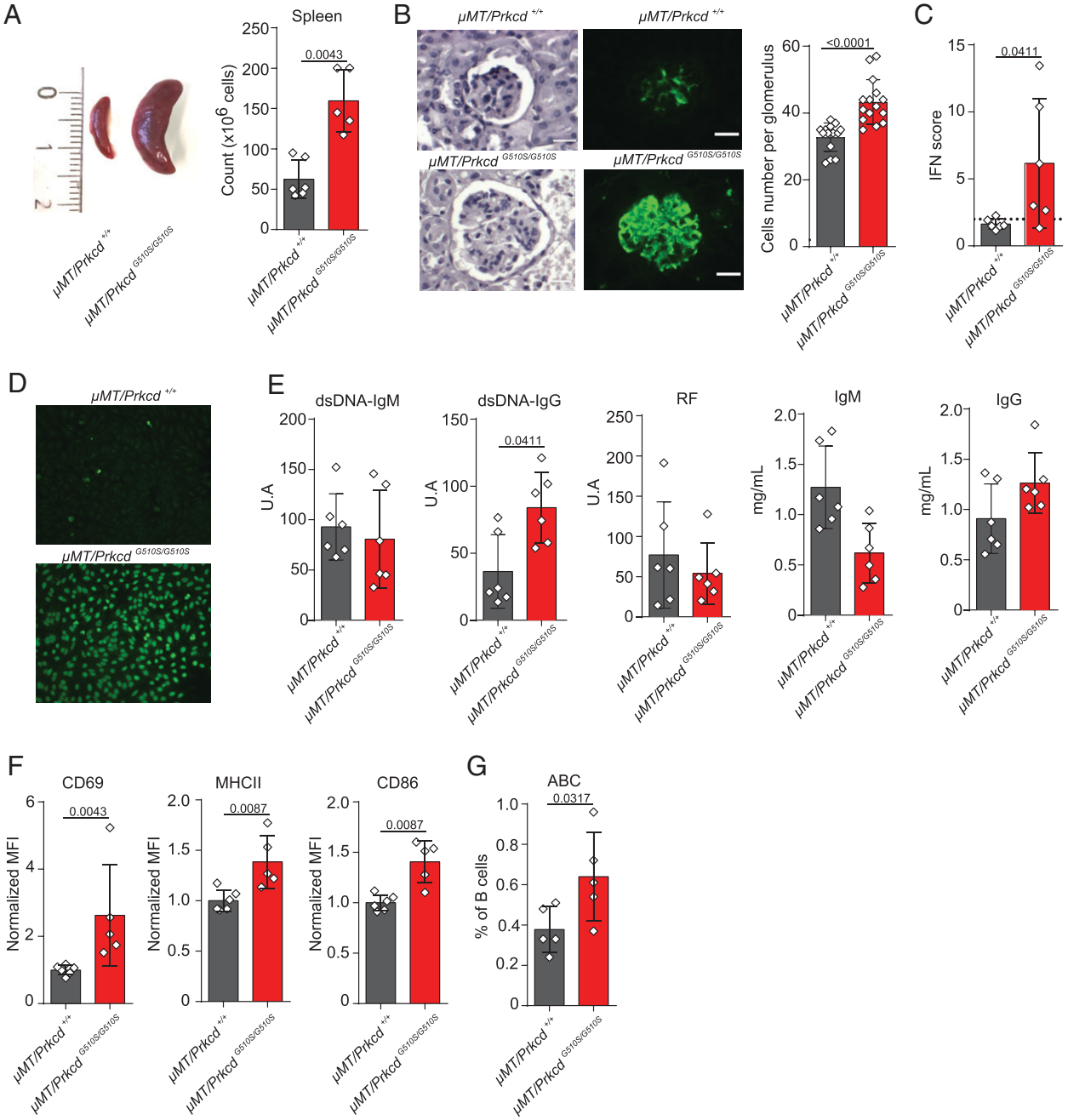

FIGURE 3. B cell–autonomous role of the *Prkcd*$^{G510S/G510S}$ mutation in autoimmunity. Mixed BM chimeras were generated by reconstituting mice with a 4:1 mixture of BM from μMT mice and BM from WT or *Prkcd*$^{G510S/G510S}$ mice. (**A**) Spleen size and cell number in spleen of *μmt/Prkcd*$^{+/+}$ and *μmt/Prkcd*$^{G510S/G510S}$ mice (n = 5–6). Statistical test: Mann–Whitney. (**B**) H&E staining (left) and immunofluorescence staining with anti–mouse IgG Ab (right) of kidney sections of the indicated mice (original magnification ×40). Numeration of glomeruli-infiltrating cells in the glomeruli based on kidney sections stained with H&E of the indicated mice. Five glomeruli per mouse were analyzed (n = 3). (**C**) IFN score in blood cells of the indicated mice (n = 6). Statistical test: Mann–Whitney. (**D**) Detection of ANAs by labeling Hep2 cells with serum from the indicated mice. (**E**) Quantification of dsDNA-IgG, RF, IgM, and IgG by ELISA in serum from the indicated mice. (**F**) Flow cytometry measurement of CD69, MHCII, and CD80 mean fluorescence intensity (MFI) normalized to WT in gated B cells from spleen of the indicated mice. (**G**) Flow cytometry analysis of ABC percentages of the indicated mice. For each group, n = 6; statistical test: Mann–Whitney. The chimeric mice (n = 5–6 for each genotype in two independent experiments) were analyzed 12 wk posttransplantation. Scale bars, 20 μm. Data are presented as the mean ± SD; no mark indicates lack of statistical significance.

autoimmunity. Notably, MZ B cells were also increased in the *Prkcd*$^{G510S/G510S}$ compartment of BM chimeric mice compared with controls (Fig. 2J), which did not correspond to the phenotype of *Prkcd*$^{G510S/G510S}$ mice. This suggests that the reduction of MZ B cells in *Prkcd*$^{G510S/G510S}$ mice was not due to a cell-intrinsic role of PKC-δ in these cells.

B cell–autonomous role of the Prkcd$^{G510S/G510S}$ *mutation in the autoimmune phenotype*

Analyses of immune subsets in *Prkcd*$^{G510S/G510S}$ mice point toward an important role of B cells in driving the autoimmune phenotype. To test whether this role was B cell autonomous, we generated mixed BM chimeric mice using a 4:1 ratio of BM from the B

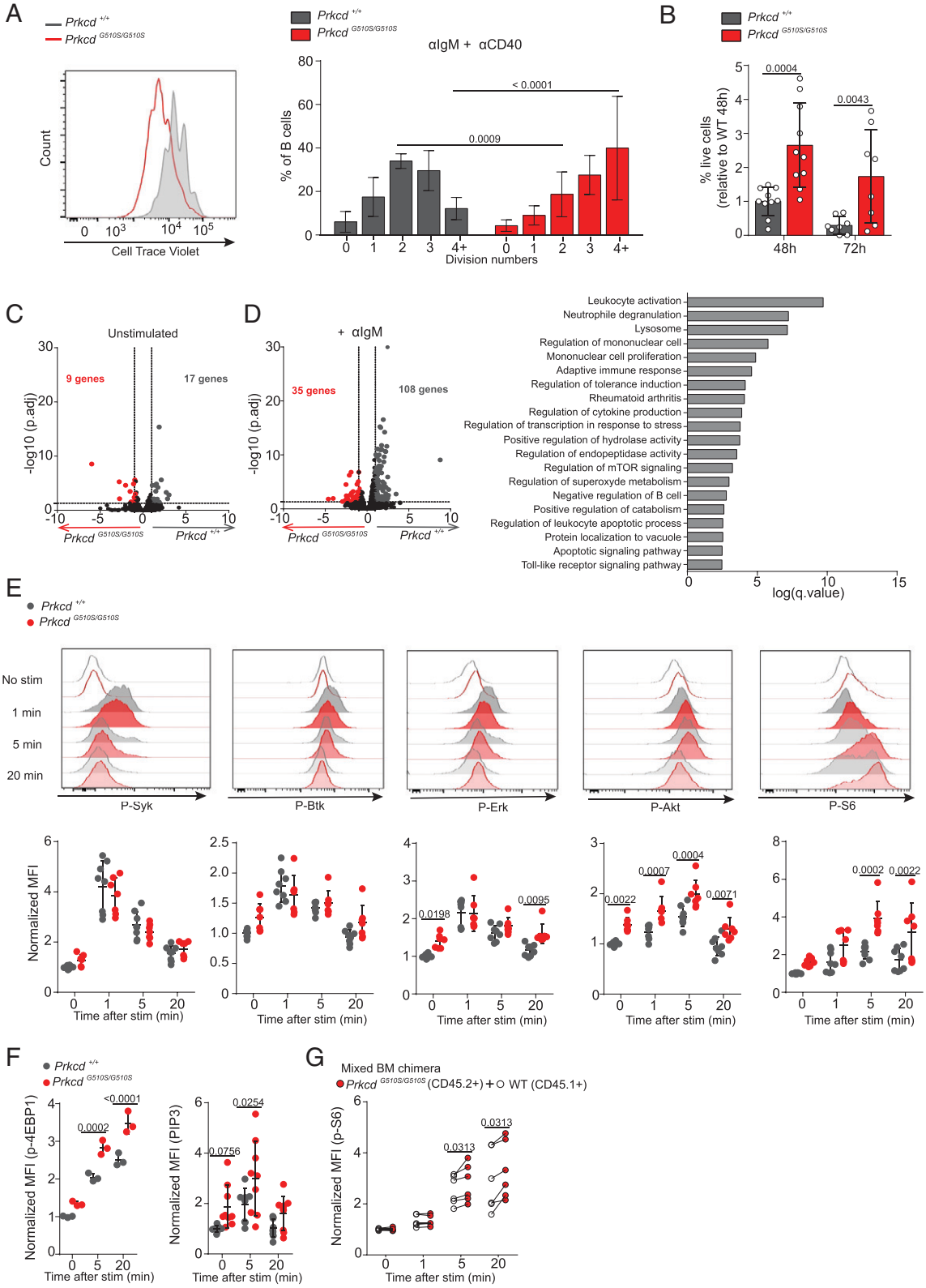

FIGURE 4. Elevated PI3K/AKT/mTOR signaling in B cells with *Prkcd*$^{G510S/G510S}$ mutation. (**A**) Flow cytometry analysis of B cell proliferation on stimulation with anti-IgM and anti-CD40 Abs, as measured by CTV dilution. Left, Representative histograms. Right, Percentage of B cells in each division round (n = 13, data pooled from four independent experiments). Statistical test: Bonferroni multiple comparisons. (**B**) Flow cytometry analysis of B cell viability after in vitro culture without stimulation. Results are normalized to the WT condition at the 48-h time point (n = 8 in two independent experiments). Statistical test: Mann–Whitney. (**C**) RNA sequencing analysis of gene transcription of *Prkcd*$^{+/+}$ and *Prkcd*$^{G510S/G510S}$ B cells at basal state or 4 h after BCR stimulation (n = 3 per group). Volcano plots of differential expression and p value are shown. Genes significantly upregulated or downregulated in *Prkcd*$^{G510S/G510S}$ B cells are shown in red and in gray, respectively (p value threshold = 0.05). (**D**) Functional annotation of DEGs between groups on BCR stimulation using Metascape. Bar graphs show selected terms among the most significant ones. (**E–G**) Flow cytometry analysis of different phosphorylation events in gated B cells from the spleen of *Prkcd*$^{+/+}$, *Prkcd*$^{G510S/G510S}$, or BM chimera mice after stimulation with anti-IgM Abs for different times. (E) Representative FACS histogram plots (top) and dot plots (one dot = one mouse bottom) of mean fluorescence intensity (MFI) of p-Syk, p-Btk, p-Erk, *(Figure legend continues)*

cell–deficient mice μMT and *Prkcd*$^{+/+}$ or *Prkcd*$^{G510S/G510S}$ mice. In those chimeric mice, most peripheral immune cells are derived from the μMT donor, except B cells that are derived only from the *Prkcd*$^{+/+}$ or the *Prkcd*$^{G510S/G510S}$ donors. Autoimmune features and immune subsets were analyzed 3 mo after BM injection. We first measured PKC-δ expression in B cells. PKC-δ expression was much lower in B cells from μMT: *Prkcd*$^{G510S/G510S}$ than in those from μMT: *Prkcd*$^{+/+}$ chimeric mice, whereas its expression was comparable in other immune cells from both mice validating the models (Supplemental Fig. 5C). Moreover, μMT: *Prkcd*$^{G510S/G510S}$ and not μMT: *Prkcd*$^{+/+}$ mice developed an autoimmune phenotype very similar to that of *Prkcd*$^{G510S/G510S}$ mice in terms of splenomegaly, glomerulonephritis, IgG deposits, IFN score, and serum antinuclear and anti-dsDNA IgG (Fig. 3A–E). Notably, some autoimmune features such as the RF, the anti-dsDNA IgM, and total Igs were more moderate in these chimeric mice compared with *Prkcd*$^{G510S/G510S}$ mice, suggesting that other cells than B cells may influence the phenotype. Yet, for the most part, the autoimmune phenotype was recapitulated in those mice, demonstrating a B cell–autonomous role of the *Prkcd*$^{G510S/G510S}$ mutation in driving B cell tolerance break and autoimmunity. We also examined B cell phenotype and activation status. B cells from μMT: *Prkcd*$^{G510S/G510S}$ displayed significantly higher levels of activation markers CD69, MHCII, and CD86 than B cells from μMT: *Prkcd*$^{+/+}$ chimeric mice (Fig. 3F). In addition, the proportion of ABCs was significantly increased in μMT: *Prkcd*$^{G510S/G510S}$ chimeric mice than was observed in *Prkcd*$^{G510S/G510S}$ mice (Fig. 3G). Thus, these results reinforce our conclusion on a cell-intrinsic role of the *Prkcd*$^{G510S/G510S}$ mutation in B cells and highlight that B cells with the *Prkcd*$^{G510S/G510S}$ mutation are sufficient to drive autoimmunity.

BCR engagement drives higher PI3K/mTOR activation and proliferation in Prkcd$^{G510S/G510S}$ *B cells than in control B cells*

We then dissected the mechanism driving autoimmune B cell activation in *Prkcd*$^{G510S/G510S}$ mice. Considering the splenomegaly and the B cell overproliferation in these mice, and the previous literature on *Prkcd*$^{-/-}$ mice, we hypothesized that *Prkcd*$^{G510S/G510S}$ B cells responded more than control B cells to BCR engagement. To test this point, we labeled splenic B cells with CTV and stimulated them with anti-IgM$^{+/-}$ anti-CD40 crosslinking Abs for 3 d. *Prkcd*$^{G510S/G510S}$ B cells proliferated more than control B cells (Fig. 4A, Supplemental Fig. 5D). Specifically, *Prkcd*$^{G510S/G510S}$ B cells performed more than four division cycles, whereas control B cells divided only twice on average on stimulation by anti-IgM and anti-CD40 Abs. By contrast, *Prkcd*$^{G510S/G510S}$ and control B cells responded equally well to LPS stimulation (Supplemental Fig. 5E), indicating a specific hyperreactivity of *Prkcd*$^{G510S/G510S}$ B cells to BCR-mediated stimulation. This phenotype was also associated to a better survival of *Prkcd*$^{G510S/G510S}$ B cells than control B cells to growth factor deprivation (Fig. 4B).

In a first attempt to understand how *Prkcd*$^{G510S/G510S}$ dysregulated B cell activation, we performed RNA sequencing on sorted *Prkcd*$^{+/+}$ and *Prkcd*$^{G510S/G510S}$ follicular B cells stimulated or not through their BCR. Although the transcriptional profile of resting *Prkcd*$^{+/+}$ and *Prkcd*$^{G510S/G510S}$ follicular B cells was relatively similar, there were greater differences between cells of both genotypes after BCR-mediated activation, with 143 differentially expressed genes (DEGs) (Fig. 4C). A functional annotation of these DEGs using Metascape (Fig. 4D) retrieved pathways related to cellular activation (leukocyte activation, mononuclear cell proliferation, etc.) confirming the impact of the *Prkcd*$^{G510S/G510S}$ mutation on B cell activation. The mTOR-signaling pathway was also differentially regulated between both cell types, pointing to a link between mTOR and PKC-δ. To substantiate this link, we analyzed signal transduction downstream of the BCR in *Prkcd*$^{G510S/G510S}$ versus *Prkcd*$^{+/+}$ B cells using phospho-specific Abs and flow cytometry, focusing on the major players of this pathway. Syk and Btk were phosphorylated at similar levels and following similar kinetics in B cells of both genotypes after BCR stimulation (Fig. 4E). However, baseline phosphorylation levels tended to be higher in *Prkcd*$^{G510S/G510S}$ B cells. ERK phosphorylation was also higher in *Prkcd*$^{G510S/G510S}$ B cells than in control B cells at baseline but also after BCR stimulation, especially at the latest time points. These results contrasted with a previous study where *Prkcd*$^{-/-}$ B cells displayed lower ERK phosphorylation than controls on thapsigargin stimulation (20, 29). To test whether the discrepancy was explained by the difference in the stimulation mode, we used thapsigargin to stimulate B cells, but a higher ERK phosphorylation was also observed in *Prkcd*$^{G510S/G510S}$ B cells in these conditions (Supplemental Fig. 5F). We then assessed activation of the mTOR pathway after BCR engagement. Basal phosphorylation levels of classical mTOR targets Akt (p-Akt), S6 (pS6), and 4EBP1 were higher in *Prkcd*$^{G510S/G510S}$ B cells compared with controls and remained significantly higher on BCR stimulation, indicating higher mTOR activity in *Prkcd*$^{G510S/G510S}$ B cells than in control B cells (Fig. 4E, 4F). Because the mTOR kinase is activated by PI3K on conversion of phosphatidylinositol (4,5)-bisphosphate into PIP3, we then measured PI3K activation on BCR engagement using a PIP3-specific Ab. PIP3 levels increased earlier than mTOR activity on BCR engagement, and their levels were higher in *Prkcd*$^{G510S/G510S}$ B cells than in control B cells (Fig. 4F). We also evaluated mTOR activation after BCR engagement in B cells from Ly5a:*Prkcd*$^{G510S/G510S}$ BM chimeric mice by measuring S6 phosphorylation. PS6 levels were higher in CD45.2^{+} *Prkcd*$^{G510S/G510S}$ B cells compared with CD45.1^{+} WT B cells (Fig. 4G), confirming the B cell–intrinsic role of the *Prkcd*$^{G510S/G510S}$ mutation in regulating the PI3K/mTOR pathway. Collectively, our results indicate that BCR engagement induces higher PI3K/mTOR activation and proliferation in *Prkcd*$^{G510S/G510S}$ B cells than in control B cells.

Rapamycin treatment reduces disease activity in Prkcd$^{G510S/G510S}$ *mice*

Based on the earlier characterization of BCR signaling in *Prkcd*$^{G510S/G510S}$ B cells, we treated *Prkcd*$^{G510S/G510S}$ and control mice with the mTORC1 inhibitor rapamycin or vehicle for 28 d (Fig. 5A). Rapamycin controlled lymphoproliferation in *Prkcd*$^{G510S/G510S}$ mice, reducing the spleen size to nearly WT levels (Fig. 5B). IgG and IgM deposits in kidneys also decreased on rapamycin treatment (Fig. 5C). Specifically, the level of IgG deposits was almost halved in rapamycin-treated mice. The IFN score

p-Akt, and p-S6 stainings in *Prkcd*$^{G510S/G510S}$ versus WT B cells, normalized to the unstimulated WT condition (bottom) ($n = 6$, data pooled from two independent experiments). Statistical test: Bonferroni multiple comparisons. (F) Dot plots of MFI of 4EBP-1 and PIP3 stainings in *Prkcd*$^{G510S/G510S}$ versus WT B cells, normalized to the unstimulated WT ($n = 3$–9 in one to three independent experiments). Statistical test: Bonferroni multiple comparisons. (G) Dot plots of MFI of pS6 staining in gated CD45.1^{+} and CD45.2^{+} B cells from BM chimera mice (CD45.1 WT/CD45.2 *Prkcd*$^{G510S/G510S}$) normalized to the unstimulated WT condition ($n = 3$–9 in one to three independent experiments). Connecting lines between dots indicate that the corresponding B cells were from the same chimeric mouse. Statistical test: Wilcoxon matched-pairs signed rank. The chimeric mice ($n = 4$ for each genotype) were analyzed 8–12 wk posttransplantation. Data are presented as the mean ± SD; no marks indicate lack of statistical significance.

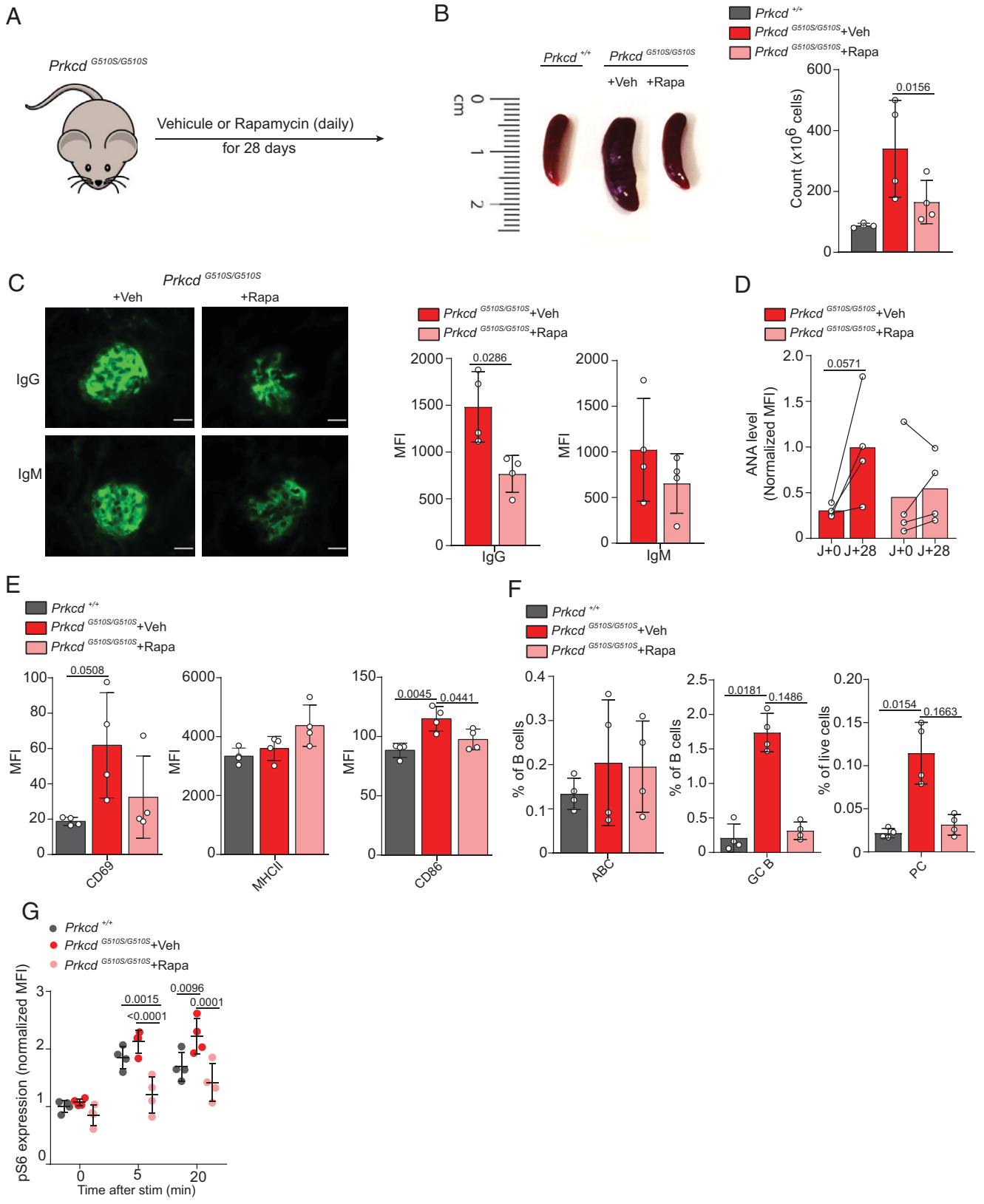

FIGURE 5. Improvement of autoimmune manifestations in *Prkcd*$^{G510S/G510S}$ mice on rapamycin treatment. (**A**) Outline of the experiment showing how *Prkcd*$^{G510S/G510S}$ mice were treated. Mice were 8–9 wk old at the beginning of treatment and were analyzed after 28 days of vehicle or rapamycin treatment (**B**) Left, Photographs of representative spleens of *Prkcd*$^{+/+}$ and *Prkcd*$^{G510S/G510S}$ mice treated with vehicle (+veh) or rapamycin (+rapa). Right, Spleen cell numbers in the different groups ($n = 4$ in each group). Statistical test: Tukey multiple comparisons. (**C**) Immunofluorescence microscopy analysis of IgG and IgM deposits in kidneys. Left, Representative photographs (original magnification ×40). Right, Quantification of the staining in the different groups. Statistical test: Mann–Whitney. (**D**) Detection of ANAs by labeling Hep2 cells with mouse serum. Analyses were made before and after treatment with rapamycin or vehicle, as indicated, and mean fluorescence intensity was quantified. Statistical test: Wilcoxon matched-pairs signed rank. (**E**) Flow cytometry measurement of CD69, MHCII, and CD80 mean fluorescence intensity (MFI) in gated B cells from spleen of the indicated mice *(Figure legend continues)*

increased over time after treatment, and there was no difference between vehicle and rapamycin groups (Supplemental Fig. 6). We also monitored serum ANA levels (Fig. 5D). We observed a global increase of ANA level in vehicle-treated mice, whereas the rapamycin treatment prevented it. Next, we examined the effect of rapamycin treatment on B cell phenotype and activation status. *Prkcd*$^{G510S/G510S}$ B cells displayed lower CD69 and CD86 activation markers in the rapamycin group compared with the vehicle group, and their levels were close to those of WT B cells (Fig. 5E). In addition, the proportions of plasma cells and GC B cells were normalized by rapamycin treatment. Aging B cells were not significantly increased in the young *Prkcd*$^{G510S/G510S}$ mice used in this experiment (Fig. 5F). Rapamycin treatment also decreased mTOR activity in *Prkcd*$^{G510S/G510S}$ B cells, close to the control levels, both at basal state and after BCR engagement (Fig. 5G). Altogether, these data demonstrate the effectiveness of rapamycin as a specific treatment of autoimmunity linked to *Prkcd* mutations.

Discussion

Since 2013, 17 patients with autosomal recessive PKC-δ deficiency have been described (6–12, 16, 24–26). In many cases, these patients suffered from typical SLE often associated with lupus nephritis and lymphoproliferation or other autoimmune manifestations. In the familial form associated with *PRKCD* G510S mutations that we previously described (6), all three patients had lupus nephritis and various autoantibodies, while two had skin involvement and other autoimmune manifestations, including arthritis, hepatomegaly, and neurological involvement for one patient and autoimmune anemia, thrombocytopenia, antiphospholipid syndrome, and lymphoproliferative disease for the other, most severe patient. To our knowledge, the novel mouse model bearing homozygous *Prkcd* G510S mutations that we present in this article essentially recapitulates the SLE features, including glomerulonephritis associated with IgG deposits, splenomegaly, and serum autoantibodies. Moreover, mice had a reduced lifespan, which correlates with the premature death of one of the patients with PRKCD G510S mutation. *Prkcd*$^{G510S/G510S}$ mice are a near phenocopy of previously described *Prkcd*$^{-/-}$ mice (13, 14). However, there is residual expression of PKC-δ protein in *Prkcd*$^{G510S/G510S}$ mice, and one cannot exclude a contribution of this mutated protein to the autoimmune phenotype. Moreover, knockout constructs can sometimes generate artifactual results by modifying expression patterns of adjacent genes or the sequence of noncoding structural elements in the genome. Thus, the point mutant mouse model we describe in this article represents a more reliable model of the human disease than the knockout mouse.

PKC-δ–deficient patients also display variable levels of immune deficiency, associated with susceptibility to bacterial, fungal, or viral infections. Chronic EBV or CMV infection has been reported (7). One of our patients also presented at the age of 30 y with severe papillomatosis caused by human papillomavirus infection (2). A previous study reported a decrease in NK cells and in their cytotoxic activity in one patient with PKC-δ deficiency. However, a decrease in peripheral NK cell numbers is often observed in SLE patients, especially when the disease is active (30). We report in this article that *Prkcd*$^{G510S/G510S}$ mice have a specific decrease in mature NK cells, and that this deficiency is caused by a role of PKC-δ in NK cell development and maturation. Although further studies will be needed to understand the precise role of PKC-δ in NK cells, a deficiency in mature NK cells can contribute to the susceptibility to viral infections in patients, as shown in mouse models (31).

We show that the autoimmune phenotype in *Prkcd*$^{G510S/G510S}$ mice is due to a B cell–autonomous impact of the Prkcd G510S mutation, confirming previous studies that used PKC-δ knockout mice (13) and pointing to PKC-δ as an important player in B cell central tolerance. Our data using the mouse model do not exclude that T cells may contribute to lupus pathology in patients as previously proposed (32, 33), but they demonstrate that the mutation in T cells is not essential for the development of the disease.

Multiple B cell subsets were altered in Prkcd$^{G510S/G510S}$ mice, with the most dramatic effect on MZ, GC, and plasma cells, the latter two expanding in the mice, which is evocative of ongoing autoimmune GC reactions. B cell tolerance mechanisms ensure that B cells with high avidity for self-antigens are eliminated in the BM. Central tolerance of B cells operates via two distinct mechanisms, which are BCR editing and clonal deletion, with BCR editing being the predominant route. BCR editing is induced in immature B lymphocytes, which express an autoreactive BCR in the BM. This mechanism operates only if the tonic signal emanating from the BCR is weak, because the recombination machinery and in particular the RAG1/2 enzymes are repressed by a strong tonic signal. Moreover, strong tonic signaling also dampens the BM retention mechanism in immature B cells. In transgenic mouse models, expression of the protein N-Ras-D12 that constitutively activates Erk1/2 phosphorylation, or expression of a constitutively active form of PI3Kδ suppresses BCR editing in autoreactive B cells, which leads to a failure of central tolerance (5). The results we present here support a model by which PKC-δ is a negative regulator of BCR signaling, especially important to limit ERK phosphorylation and PI3K/mTOR activation. In particular, Prkcd$^{G510S/G510S}$ B cells display elevated basal levels of p-Akt, pS6, and pERK, evocative of strong tonic BCR signaling. This higher tonic signaling may therefore prevent BCR editing in autoreactive clones, which would result in B cell tolerance break and autoimmunity. Notably, a previous article reported a decrease in Erk phosphorylation on thapsigargin stimulation in PKC-δ–deficient B cells (20–22, 24–29). We also used thapsigargin in our study but obtained opposite results, i.e., Prkcd$^{G510S/G510S}$ B cells displayed stronger ERK phosphorylation after stimulation with thapsigargin. Technical differences may explain this discrepancy, but our results were supported by a comprehensive analysis of other BCR signaling branches that matched with the p-Erk data. Previous reports also showed that PKC-δ was essential for B cell tolerance by shuttling to the nucleus and inducing apoptosis on BCR engagement to induce clonal deletion (21). Our observation that *Prkcd*$^{G510S/G510S}$ B cells survive better than control B cells during in vitro cultures are in agreement with this possibility. PKC-δ could therefore have several roles in B cell tolerance by promoting both clonal deletion and BCR editing in immature cells. Further studies will be required to determine the conditions that allow each of these PKC-δ functions and how they are coordinated during B cell development.

Mature B cells in the periphery of *Prkcd*$^{G510S/G510S}$ mice displayed higher proliferation than controls on BCR engagement, a phenotype also observed in *Prkcd*$^{-/-}$ mice (13) and in PKC-δ–deficient patients (7). Mechanistically, we linked this hyperreactivity to unrestrained BCR signaling, in particular at the level of the PI3K/mTOR

($n = 4$ in each group). Statistical test: Tukey multiple comparisons. (**F**) Flow cytometry analysis of ABCs, GC B cells, and PC cells percentages of the indicated mice. Statistical test: Tukey multiple comparisons. (**G**) Flow cytometry measurement of P-S6 MFI normalized on unstimulated WT in gated B cells from spleen after treatment with anti-IgM of the indicated mice. Statistical test: Tukey multiple comparisons. Data are presented as the mean ± SD; no marks indicate lack of statistical significance.

pathway. This pathway is known to have multiple roles in mature B cells, promoting survival, proliferation, and differentiation of activated B cells (34). In particular, the reduced survival of mature BCR-deficient B cells can be rescued by activation of PI3K signaling (35). In agreement with our findings, gain-of-function mutations in the *PIK3CD* gene encoding the catalytic subunit p110d of PI3K cause activated-PI3K-d syndrome that combines massive lymphoproliferation with immunodeficiency and/or autoimmune features. Although this phenotype resembles that of PKC-δ deficiency, a recent article that reviewed genetic defects associated with an autoimmune lymphoproliferative phenotype found highest correspondence in terms of clinical features and immunophenotyping between PKC-δ deficiency and Ras-associated lymphoproliferative diseases (RALDs) (36). RALD is caused by somatic activating mutations in *KRAS* or *NRAS* that appear in hematopoietic progenitor or stem cells and are subsequently detectable in lymphocytes and monocytes (37). RALD presents with B cell lymphocytosis and may present with laboratory and clinical features not seen in patients with autoimmune lymphoproliferative syndrome because of *FAS* mutations such as SLE-like autoimmunity. Ras mediates the cellular response to growth factors, which leads to modulation of gene expression necessary for cell growth and proliferation. Ras operates through multiple downstream effectors, including PI3K and mTORC2 (38), and PKC-δ has been proposed to be an effector of oncogenic Ras in lung tumors (39). In B cells, Ras is activated downstream of BCR engagement through the guanine nucleotide exchange factors RasGRP1 and RasGRP3 (29). Further studies will be needed to clarify the link between PKC-δ and the activation of Ras in B cells, and more broadly to the 22 proteins whose defect have been associated with autoimmune lymphoproliferative syndrome-like disorders (36). Moreover, how PKC-δ negatively regulates mTOR activity in BCR-stimulated B cells remains to be determined considering that in other cellular pathways, PKC-δ has been shown to activate mTOR, in particular through TSC2 phosphorylation (40).

Despite the knowledge gained on the role of PKC-δ in immune regulation, no specific treatment was identified for *PRKCD*-mutated patients thus far. Such treatments may benefit a broader group of patients because PKC-δ expression appears to be silenced in PBMCs from adult-onset lupus patients (41). Based on the in vitro evidence of strong PI3K/mTOR activation in $Prkcd^{G510S/G510S}$ B cells, we selected rapamycin as a specific treatment of autoimmune features in $Prkcd^{G510S/G510S}$ mice. This strategy proved to be relevant as a 28-d daily treatment; rapamycin was sufficient to restore spleen homeostasis and alleviate autoimmune features in mice. This effectiveness correlated with a normalization of PI3K/mTOR activation in B cells after treatment. Interestingly, two patients with PRKCD deficiency received sirolimus, which corresponds to rapamycin, and showed excellent clinical response to treatment (7, 42). In addition, stopping treatment for 6 mo in one patient resulted in a significant relapse, highlighting the effectiveness of this treatment in the patient (42). Thus, and even though the usual clinical practice is to use rapamycin to treat lymphoproliferative disorders, our translational study provides a strong rationale to do it when the cause of the disease is proven to be PKC-δ deficiency.

Acknowledgments

We acknowledge the contribution of the SFR Biosciences (UAR3444/CNRS, US8/INSERM, ENS de Lyon, UCBL) facilities: ANIRA-PBES, ANIRA-Cytométrie, PSF, and ANIRA-AGC.

Disclosures

The authors have no financial conflicts of interest.

References

1. Belot, A., G. I. Rice, S. O. Omarjee, Q. Rouchon, E. M. D. Smith, M. Moreews, M. Tusseau, C. Frachette, R. Bournhonesque, N. Thielens, et al. 2020. Contribution of rare and predicted pathogenic gene variants to childhood-onset lupus: a large, genetic panel analysis of British and French cohorts. *Lancet Rheumatol.* 2: e99–e109.
2. Omarjee, O., C. Picard, C. Frachette, M. Moreews, F. Rieux-Laucat, P. Soulas-Sprauel, S. Viel, J.-C. Lega, B. Bader-Meunier, T. Walzer, et al. 2019. Monogenic lupus: dissecting heterogeneity. *Autoimmun. Rev.* 18: 102361.
3. Tsokos, G. C., M. S. Lo, P. Costa Reis, and K. E. Sullivan. 2016. New insights into the immunopathogenesis of systemic lupus erythematosus. *Nat. Rev. Rheumatol.* 12: 716–730.
4. Cashman, K. S., S. A. Jenks, M. C. Woodruff, D. Tomar, C. M. Tipton, C. D. Scharer, F. Eun-Hyung Lee, J. M. Boss, and I. Sanz. 2019. Understanding and measuring human B-cell tolerance and its breakdown in autoimmune disease. *Immunol. Rev.* 292: 76–89.
5. Pelanda, R., S. A. Greaves, T. Alves da Costa, L. M. Cedrone, M. L. Campbell, and R. M. Torres. 2022. B-cell intrinsic and extrinsic signals that regulate central tolerance of mouse and human B cells. *Immunol. Rev.* 307: 12–26.
6. Belot, A., P. R. Kasher, E. W. Trotter, A.-P. Foray, A.-L. Debaud, G. I. Rice, M. Szynkiewicz, M.-T. Zabot, I. Rouvet, S. S. Bhaskar, et al. 2013. Protein kinase cδ deficiency causes mendelian systemic lupus erythematosus with B cell-defective apoptosis and hyperproliferation. *Arthritis Rheum.* 65: 2161–2171.
7. Kuehn, H. S., J. E. Niemela, A. Rangel-Santos, M. Zhang, S. Pittaluga, J. L. Stoddard, A. A. Hussey, M. O. Evbuomwan, D. A. L. Priel, D. B. Kuhns, et al. 2013. Loss-of-function of the protein kinase C δ (PKCδ) causes a B-cell lymphoproliferative syndrome in humans. *Blood* 121: 3117–3125.
8. Salzer, E., E. Santos-Valente, S. Klaver, S. A. Ban, W. Emminger, N. K. Prengemann, W. Garncarz, L. Müllauer, R. Kain, H. Boztug, et al. 2013. B-cell deficiency and severe autoimmunity caused by deficiency of protein kinase C δ. *Blood* 121: 3112–3116.
9. Kiykim, A., I. Ogulur, S. Baris, E. Salzer, E. Karakoc-Aydiner, A. O. Ozen, W. Garncarz, T. Hirschmugl, A. Krolo, A. D. Yucelten, et al. 2015. Potentially beneficial effect of hydroxychloroquine in a patient with a novel mutation in protein kinase Cδ deficiency. *J. Clin. Immunol.* 35: 523–526.
10. Nanthapisal, S., E. Omoyinmi, C. Murphy, A. Standing, M. Eisenhut, D. Eleftheriou, and P. A. Brogan. 2017. Early-onset juvenile SLE associated with a novel mutation in protein kinase C δ. *Pediatrics* 139: e20160781.
11. Lei, L., S. Muhammad, M. Al-Obaidi, N. Sebire, I. L. Cheng, D. Eleftheriou, and P. Brogan. 2018. Successful use of ofatumumab in two cases of early-onset juvenile SLE with thrombocytopenia caused by a mutation in protein kinase C δ. *Pediatr. Rheumatol. Online J.* 16: 61.
12. Sharifinejad, N., G. Azizi, N. Behniafard, M. Zaki-Dizaji, M. Jamee, R. Yazdani, H. Abolhassani, and A. Aghamohammadi. 2022. Protein kinase C-delta defect in autoimmune lymphoproliferative syndrome-like disease: first case from the National Iranian Registry and review of the literature. *Immunol. Invest.* 51: 331–342.
13. Miyamoto, A., K. Nakayama, H. Imaki, S. Hirose, Y. Jiang, M. Abe, T. Tsukiyama, H. Nagahama, S. Ohno, S. Hatakeyama, and K. I. Nakayama. 2002. Increased proliferation of B cells and auto-immunity in mice lacking protein kinase Cdelta. *Nature* 416: 865–869.
14. Mecklenbräuker, I., K. Saijo, N.-Y. Zheng, M. Leitges, and A. Tarakhovsky. 2002. Protein kinase Cdelta controls self-antigen-induced B-cell tolerance. *Nature* 416: 860–865.
15. Kilpatrick, L. E., S. Sun, H. Li, T. C. Vary, and H. M. Korchak. 2010. Regulation of TNF-induced oxygen radical production in human neutrophils: role of δ-PKC. *J. Leukoc. Biol.* 87: 153–164.
16. Neehus, A.-L., K. Moriya, A. Nieto-Patlán, T. Le Voyer, R. Lévy, A. Özen, E. Karakoc-Aydiner, S. Baris, A. Yildiran, E. Altundag, et al. 2021. Impaired respiratory burst contributes to infections in PKCδ-deficient patients. *J. Exp. Med.* 218: e20210501.
17. Parihar, S. P., M. Ozturk, M. J. Marakalala, D. T. Loots, R. Hurdayal, D. B. Maasdorp, M. Van Reenen, D. E. Zak, F. Darboe, A. Penn-Nicholson, et al. 2018. Protein kinase C-delta (PKCδ), a marker of inflammation and tuberculosis disease progression in humans, is important for optimal macrophage killing effector functions and survival in mice. [Published erratum appears in 2018 *Mucosal Immunol.* 11: 579–580.] *Mucosal Immunol.* 11: 496–511 .
18. Pracht, C., S. Minguet, M. Leitges, M. Reth, and M. Huber. 2007. Association of protein kinase C-δ with the B cell antigen receptor complex. *Cell. Signal.* 19: 715–722.
19. Popoff, I. J., and J. P. Deans. 1999. Activation and tyrosine phosphorylation of protein kinase C δ in response to B cell antigen receptor stimulation. *Mol. Immunol.* 36: 1005–1016.
20. Limnander, A., J. Zikherman, T. Lau, M. Leitges, A. Weiss, and J. P. Roose. 2014. Protein kinase Cδ promotes transitional B cell-negative selection and limits proximal B cell receptor signaling to enforce tolerance. *Mol. Cell. Biol.* 34: 1474–1485.
21. Mecklenbräuker, I., S. L. Kalled, M. Leitges, F. Mackay, and A. Tarakhovsky. 2004. Regulation of B-cell survival by BAFF-dependent PKCdelta-mediated nuclear signalling. *Nature* 431: 456–461.
22. Ou, P., A. Stanek, Z. Huan, C. A. J. Roman, and C. Huan. 2021. SMS2 deficiency impairs PKCδ-regulated B cell tolerance in the germinal center. *Cell Rep.* 36: 109624.
23. Teixeira, M., B. F. Py, C. Bosc, D. Laubreton, M.-J. Moutin, J. Marvel, F. Flamant, and S. Markossian. 2018. Electroporation of mice zygotes with dual guide RNA/Cas9 complexes for simple and efficient cloning-free genome editing. [Published erratum appears in 2018 *Sci. Rep.* 8: 4679.] *Sci. Rep.* 8: 474.

24. Meyts, I., G. Bucciol, I. Quinti, B. Neven, A. Fischer, E. Seoane, E. Lopez-Granados, C. Gianelli, A. Robles-Marhuenda, P.-Y. Jeandel, et al; IUIS Committee of Inborn Errors of Immunity. 2021. Coronavirus disease 2019 in patients with inborn errors of immunity: an international study. *J. Allergy Clin. Immunol.* 147: 520–531.
25. Roderick, M. R., L. Jefferson, W. Renton, and A. Belot; PRKCD Consortium. 2023. Compound heterozygous mutations in PRKCD associated with early-onset lupus and severe and invasive infections in siblings. *J. Clin. Immunol.* DOI: 10.1007/s10875-022-01416-0.
26. Neehus, A.-L., K. Tuano, T. Le Voyer, S. L. Nandiwada, K. Murthy, A. Puel, J.-L. Casanova, J. Chinen, and J. Bustamante. 2022. Chronic granulomatous disease-like presentation of a child with autosomal recessive PKCδ deficiency. *J. Clin. Immunol.* 42: 1244–1253.
27. Pescarmona, R., A. Belot, M. Villard, L. Besson, J. Lopez, I. Mosnier, A.-L. Mathieu, C. Lombard, L. Garnier, C. Frachette, et al. 2019. Comparison of RT-qPCR and Nanostring in the measurement of blood interferon response for the diagnosis of type I interferonopathies. *Cytokine* 113: 446–452.
28. Sachinidis, A., K. Xanthopoulos, and A. Garyfallos. 2020. Age-associated B cells (ABCs) in the prognosis, diagnosis and therapy of systemic lupus erythematosus (SLE). *Mediterr. J. Rheumatol.* 31: 311–318.
29. Limnander, A., P. Depeille, T. S. Freedman, J. Liou, M. Leitges, T. Kurosaki, J. P. Roose, and A. Weiss. 2011. STIM1, PKC-δ and RasGRP set a threshold for proapoptotic Erk signaling during B cell development. *Nat. Immunol.* 12: 425–433.
30. Henriques, A., L. Teixeira, L. Inês, T. Carvalheiro, A. Gonçalves, A. Martinho, M. L. Pais, J. A. P. da Silva, and A. Paiva. 2013. NK cells dysfunction in systemic lupus erythematosus: relation to disease activity. *Clin. Rheumatol.* 32: 805–813.
31. Biron, C. A., K. B. Nguyen, G. C. Pien, L. P. Cousens, and T. P. Salazar-Mather. 1999. Natural killer cells in antiviral defense: function and regulation by innate cytokines. *Annu. Rev. Immunol.* 17: 189–220.
32. Richardson, B., F. M. Strickland, A. H. Sawalha, and G. Gorelik. 2014. Protein kinase Cδ mutations may contribute to lupus through effects on T cells: comment on the article by Belot et al. *Arthritis Rheumatol.* 66: 228–229.
33. Sawalha, A. H., M. Jeffries, R. Webb, Q. Lu, G. Gorelik, D. Ray, J. Osban, N. Knowlton, K. Johnson, and B. Richardson. 2008. Defective T-cell ERK signaling induces interferon-regulated gene expression and overexpression of methylation-sensitive genes similar to lupus patients. *Genes Immun.* 9: 368–378.
34. Limon, J. J., and D. A. Fruman. 2012. Akt and mTOR in B cell activation and differentiation. *Front. Immunol.* 3: 228.
35. Srinivasan, L., Y. Sasaki, D. P. Calado, B. Zhang, J. H. Paik, R. A. DePinho, J. L. Kutok, J. F. Kearney, K. L. Otipoby, and K. Rajewsky. 2009. PI3 kinase signals BCR-dependent mature B cell survival. *Cell* 139: 573–586.
36. López-Nevado, M., L. I. González-Granado, R. Ruiz-García, D. Pleguezuelo, O. Cabrera-Marante, N. Salmón, P. Blanco-Lobo, N. Domínguez-Pinilla, R. Rodríguez-Pena, E. Sebastián, et al. 2021. Primary immune regulatory disorders with an autoimmune lymphoproliferative syndrome-like phenotype: immunologic evaluation, early diagnosis and management. *Front. Immunol.* 12: 671755.
37. Meynier, S., and F. Rieux-Laucat. 2019. FAS and RAS related apoptosis defects: from autoimmunity to leukemia. *Immunol. Rev.* 287: 50–61.
38. Smith, S. F., S. E. Collins, and P. G. Charest. 2020. Ras, PI3K and mTORC2—three's a crowd? *J. Cell Sci.* 133: jcs234930.
39. Ohm, A. M., A.-C. Tan, L. E. Heasley, and M. E. Reyland. 2017. Co-dependency of PKCδ and K-Ras: inverse association with cytotoxic drug sensitivity in KRAS mutant lung cancer. *Oncogene* 36: 4370–4378.
40. Zhan, J., R. K. Chitta, F. C. Harwood, and G. C. Grosveld. 2019. Phosphorylation of TSC2 by PKC-δ reveals a novel signaling pathway that couples protein synthesis to mTORC1 activity. *Mol. Cell. Biochem.* 456: 123–134.
41. Bíró, T., Z. Griger, E. Kiss, H. Papp, M. Aleksza, I. Kovács, M. Zeher, E. Bodolay, T. Csépány, K. Szûcs, et al. 2004. Abnormal cell-specific expressions of certain protein kinase C isoenzymes in peripheral mononuclear cells of patients with systemic lupus erythematosus: effect of corticosteroid application. *Scand. J. Immunol.* 60: 421–428.
42. Gu, H., Z. Chen, J. Ma, J. Wang, R. Zhang, R. Wu, and T. Wang. 2021. Sirolimus is effective in autoimmune lymphoproliferative syndrome-type III: a pedigree case report with homozygous variation PRKCD. *Int. J. Immunopathol. Pharmacol.* 35: 20587384211025934.